Hinf Controller Design for a Variable Wind Speed Turbine

H. González , H. R. Vargas

Abstract: **This paper gives a description of a wind generator system composed by a doubly fed induction generator (DFIG), its dynamic model and each one of its subsystems. Also, the control logic that regulates the active and reactive power delivered by the DFIG is described. The electrical control logic is based on stator flux oriented technique and the turbine speed is controlled varying the blade pitch angle. The three regulators found had been designed using the frequency domain approach based on genetic algorithms.**

Keywords: **wind turbine, wind model, doubly fed induction generator, stator flux oriented control, blade pitch angle control.**

I. INTRODUCTION

The dramatic growth of wind power systems has pushed research and publications about this topic around the world. South America is not an exception. The mathematic models of wind power systems with their subsystems has been treated in different doctoral thesis, [1], [2], [3], [4], addressing in more or less detail, the diverse phenomena which appear during the transformation process of wind energy in electric energy (aerodynamic, mechanic and electromagnetic phenomena).

The technology is changing the way electric power is converted from wind power. Initial projects employed turbines of constant speed and squirrel cage induction motor. Now, turbines of variable speed and doubly fed induction generator (DFIG) are being employed. The stator winding of the DFIG is interconnected to the electric network at constant frequency and the rotor winding is interconnected to a system of magnitude, phase and frequency variables. This system is composed by an AC/AC inverter that regulates the active and reactive power delivered by the DFIG to the grid in spite of fluctuating wind.

A control scheme used in DFIG is based in the oriented field control. The main advantage of this scheme is the decoupling of the DFIG dynamic. This decoupling permits to implement two independent regulators to the rotor current components: I_{dr} and I_{qr}, allowing regulate the output power too [5], [6], [7], [8], [9]. Its control logic is backed up with a system that regulates the mechanic speed of the rotor using a PI regulator which varies the blade pitch angle [10], [11], [12].

Given that certain wind turbine system parameters can change over time, new approaches based in LQG [11], Hinf [12] and adaptive control [13], among others, has been proposed. Those approaches seek to avoid dependence upon parameter variations and wind speed variations.

II. DYNAMIC MODEL OF THE WIND

The wind speed distribution over the rotor swept area can be calculated as the sum of two components at hub level: the first is the average speed and the second, called turbulence, related with the temporal variations of the wind speed but defined in frequency domain with the Kaimal spectrum [3]:

$$S_t(f) = \frac{\sigma^2}{2}\frac{L}{V_0}\frac{1}{\left(1+\frac{3}{2}\frac{L}{V_0}f\right)^{\frac{5}{3}}} \quad (1)$$

$$L = \begin{cases} 20z & to\ z < 20\ m \\ 600 & to\ z > 20\ m \end{cases} \quad (2)$$

$$\sigma = IV_o \quad (3)$$

where

- f Frequency
- L Turbulence length scale
- z Tower height
- σ Stantadard deviation of the wind speed
- I Turbulence strength
- V_o Average wind speed

To simulate the fluctuations of the wind in the time domain a white noise generator is used interconnected to an analog filter [2] that shows a power spectral density (PSD) very approximate Kaimal model and given by equation (4).

$$H(s) = \sigma\sqrt{\frac{L}{V_0}}\frac{0{,}0182c^2s^2 + 1{,}3653cs + 0{,}9846}{1{,}3463c^2s^2 + 3{,}7593cs + 1} \quad (4)$$

$$c = \frac{L}{2\pi V_0} \quad (5)$$

978-1-4244-2218-0/08/$25.00 ©2008 IEEE.

In a turbine of three blades, spaced 120 degrees, has been found that appearing fluctuations in the aerodynamic torque are produced by third order harmonic components of the turbulence, with a fundamental frequency of equal value to the speed of the rotor. This situation is known as *"rotational sampling of turbulence"* (reported as the main cause of flicker from wind turbines). The block diagram shown in figure 1 models this situation. This system generates a wind speed time series sequence located at hub level.

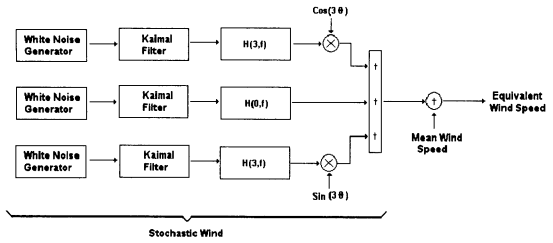

Fig. 1 Block diagram representation of the equivalent wind speed model

where θ is the turbine displacement angle. The boxes *H(0,f)* and *H(3,f)* that represent the effects of the dc and third wind speed harmonic components on turbine shaft torque respectively, are given by

$$H(0,f)=\frac{4,7869d_{TF}s+0,9904}{7,6823{d_{TF}}^2s^2+7,3518d_{TF}s+1} \quad (6)$$

$$H(3,f)=\frac{0,2766d_{TF}s+0,0307}{0,3691{d_{TF}}^2s^2+1,7722d_{TF}s+1} \quad (7)$$

$$d_{TF}=R/V_0 \quad (8)$$

where R is the turbine blade radius.

III. AERODYNAMIC ROTOR MODEL

The conversion of the wind power to mechanical power by the wind turbine rotor can be calculated by:

$$P=\frac{1}{2}\rho\, A\, \mathrm{V}^3\, C_p(\lambda,\beta) \quad (9)$$

and

$$\lambda=\frac{\omega_{Rot}R}{v} \quad (10)$$

where P is the rotor mechanical power, ρ is the air density, A is the rotor surface, V is the wind speed at the center of the rotor (Fig. 1), C_p is the rotor aerodynamic power coefficient, β is the blade pitch angle and ω_{ROT} is the turbine angular mechanical speed.

The rotor aerodynamic power coefficient C_p depends on the aerodynamic design of the turbine. Any design of wind turbine has a theoretical maximum value of 0.593, called Betz limit. C_p can be calculated using equations (11) and (12)

$$Cp=0,5176\left(\frac{116}{\lambda_i}-0,4\beta-5\right)e^{-21/\lambda_i}+0,0068\lambda \quad (11)$$

$$\frac{1}{\lambda_i}=\frac{1}{\lambda+0,08\beta}-\frac{0.035}{\beta^3+1} \quad (12)$$

IV. MECHANICAL MODEL

There are wind turbine mechanical parts such as blades, low speed shaft, gear box, high speed shaft and generator that form a mechanical system that can transmit oscillations to the grid. Such dynamic system is represented by a four mass equivalent model (Figure 2.). This model may be described as follows:

$$T_{Aer}=\frac{1}{2}\rho\, AR\frac{C_p(\lambda,\beta)}{\lambda}V^2 \quad (13)$$

$$T_{Aer}-D_{Rot}(\omega_{Rot}-\omega_1)-Q_{Rot}=J_{Rot}\frac{d}{dt}\omega_{Rot} \quad (14)$$

$$D_{Rot}(\omega_{Rot}-\omega_1)+Q_{Rot}-T_1=J_{Eng1}\frac{d}{dt}\omega_1 \quad (15)$$

$$T_2-D_{Gen}(\omega_2-\omega_{Gen})-Q_{Gen}=J_{Eng2}\frac{d}{dt}\omega_2 \quad (16)$$

$$D_{Gen}(\omega_2-\omega_{Gen})+Q_{Gen}-T_{Elec}=J_{Gen}\frac{d}{dt}\omega_{Gen} \quad (17)$$

$$Q_{Rot}=K_{Rot}\int(\omega_{Rot}-\omega_1)\,\mathrm{d}t \quad (18)$$

$$Q_{Gen}=K_{Gen}\int(\omega_2-\omega_{Gen})\,\mathrm{d}t \quad (19)$$

$$\frac{T_1}{T_2}=\frac{\omega_2}{\omega_1}=n_{Eng} \quad (20)$$

where

T_{Aer}	Aerodynamic torque
J_{Rot}	Blades and rotor hub moment of inertia
K_{Rot}	Low speed shaft tortional stiffness
D_{Rot}	Low speed shaft damping coefficient
ω_{Rot}	Turbine angular speed
J_{Eng1} J_{Eng2}	Gear boxes moment of inertia
ω_1 ω_2	Gear boxes angular speeds
n_{Eng}	Ratio gear box
K_{gen}	High speed shaft tortional stiffness
D_{gen}	High speed shaft damping coefficient

ω_{Gen} Generator angular speed
J_{Gen} Generator moment of inertia
T_{Elec} Generator electromagnetic torque

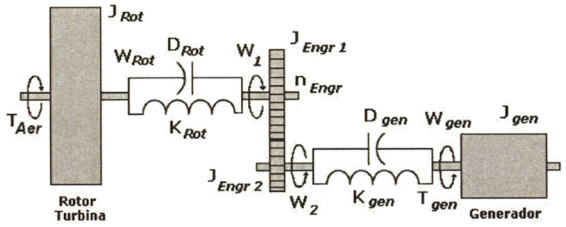

Fig. 2 Four mass mechanical equivalent

V. DFIG MODEL

Here, the doubly fed induction generator based on variable speed use induction machine model in two axis d-q reference frame rotating at ω_o synchronous speed. Beginning with stator currents, the transformation equations to d-q coordinates is given in equation (21):

$$\begin{bmatrix} I_{ds} \\ I_{qs} \end{bmatrix} = \frac{2}{3}\begin{bmatrix} \cos(\omega_o t) & \cos\left(\omega_o t - \frac{2\pi}{3}\right) & \cos\left(\omega_o t + \frac{2\pi}{3}\right) \\ -\sin(\omega_o t) & -\sin\left(\omega_o t - \frac{2\pi}{3}\right) & -\sin\left(\omega_o t + \frac{2\pi}{3}\right) \end{bmatrix}\begin{bmatrix} I_A \\ I_B \\ I_C \end{bmatrix} \tag{21}$$

To rotor currents, the transformation equations to d-q coordinates are given in equation (22):

$$\begin{bmatrix} I_{dr} \\ I_{qr} \end{bmatrix} = \frac{2}{3}\begin{bmatrix} \cos(\theta) & \cos\left(\theta - \frac{2\pi}{3}\right) & \cos\left(\theta + \frac{2\pi}{3}\right) \\ -\sin(\theta) & -\sin\left(\theta - \frac{2\pi}{3}\right) & -\sin\left(\theta + \frac{2\pi}{3}\right) \end{bmatrix}\begin{bmatrix} I_a \\ I_b \\ I_c \end{bmatrix} \tag{22}$$

where

$$\frac{d}{dt}\theta = \omega_o - \omega_r \tag{23}$$

By applying the d-q transformation, using equations (21), (22) and (23), the stator and rotor voltages equations result:

$$\begin{bmatrix} V_{ds} \\ V_{qs} \\ V_{dr} \\ V_{qr} \end{bmatrix} = [R]\begin{bmatrix} I_{ds} \\ I_{qs} \\ I_{dr} \\ I_{qr} \end{bmatrix} + \frac{d}{dt}\begin{bmatrix} \Psi_{ds} \\ \Psi_{qs} \\ \Psi_{dr} \\ \Psi_{qr} \end{bmatrix} + [\Omega]\begin{bmatrix} \Psi_{ds} \\ \Psi_{qs} \\ \Psi_{dr} \\ \Psi_{qr} \end{bmatrix} \tag{24}$$

$$R = \begin{bmatrix} R_s & 0 & 0 & 0 \\ 0 & R_s & 0 & 0 \\ 0 & 0 & R_r & 0 \\ 0 & 0 & 0 & R_r \end{bmatrix} \tag{25}$$

$$\Omega = \begin{bmatrix} 0 & -\omega_o & 0 & 0 \\ \omega_o & 0 & 0 & 0 \\ 0 & 0 & 0 & -(\omega_o - \omega_r) \\ 0 & 0 & (\omega_o - \omega_r) & 0 \end{bmatrix} \tag{26}$$

$$\begin{bmatrix} \Psi_{ds} \\ \Psi_{qs} \\ \Psi_{dr} \\ \Psi_{qr} \end{bmatrix} = \begin{bmatrix} L_{ss} & 0 & L_m & 0 \\ 0 & L_{ss} & 0 & L_m \\ L_m & 0 & L_{rr} & 0 \\ 0 & L_m & 0 & L_{rr} \end{bmatrix}\begin{bmatrix} I_{ds} \\ I_{qs} \\ I_{dr} \\ I_{qr} \end{bmatrix} \tag{27}$$

where

R_s Stator winding resistance
L_{ss} Stator winding inductance
R_r Rotor winding resistance
L_{rr} Rotor windig inductance
L_m Mutual inductance
P_f Even number of poles

The electromagnetic torque, the active and reactive power on the stator side in the d-q coordinates are given respectively as:

$$T_e = \frac{3}{2}P_f L_m \left(I_{dr} I_{qs} - I_{qr} I_{ds}\right) \tag{28}$$

$$P_{ACT} = \frac{3}{2}\left(V_{ds} I_{ds} + V_{qs} I_{qs}\right) \tag{29}$$

$$Q_{REA} = \frac{3}{2}\left(V_{qs} I_{ds} - V_{ds} I_{qs}\right) \tag{30}$$

There are two operation modes of DFIG, which depend on the magnitude and phase of rotor voltage respect to induced voltage: In the sub-synchronous operation mode, magnitude rotor voltage is greater than induced voltage magnitude, and the rotor voltage is in phase with the induced voltage. In the super-synchronous operation mode, magnitude rotor voltage is less than induced voltage magnitude, and the rotor voltage is the anti-phase with the induced voltage. In order to avoid the instability of the generation system is best to control the DIFG generated power applying rotor voltage between $0 \le V_{dr} \le \infty$ and $-\infty \le V_{qr} \le 0$, using the super-synchronous operation mode.

VI. STATOR FLUX ORIENTED CONTROL

This approach seeks to emulate the control of a direct current machine, having into account the next considerations:

- Stator resistance R_s is neglected, mainly on power machines greater than 10 kW.
- Magnetization current phasor $\left|\overline{I_{ms}}\right|$, is supposed constant.
- Grid frequency is supposed constant.

Assuming that stator flux magnitude and direction are kept constant, the magnetic flux equations, equation (27), may be expressed as

$$\Psi_{ds} = L_m\left|\overline{I_{ms}}\right| = L_{ss}I_{ds} + L_m I_{dr} \tag{31}$$

$$\Psi_{qs} = 0 = L_{ss}I_{qs} + L_m I_{qr} \tag{32}$$

$$\Psi_{dr} = \frac{L_m^2}{L_{ss}}\left|\overline{I_{ms}}\right| + \sigma L_{rr} I_{dr} \tag{33}$$

$$\Psi_{qr} = \sigma L_{rr} I_{qr} \tag{34}$$

$$\sigma = 1 - \frac{L_m^2}{L_{ss}L_{rr}} \tag{35}$$

The above equations can be used to obtain the DFIG simplified model, equations (36) and (37).

$$\begin{bmatrix} \dot{I}_{dr} \\ \dot{I}_{qr} \end{bmatrix} = \begin{bmatrix} -\frac{R_r}{\sigma L_{rr}} & \omega_{sl} \\ -\omega_{sl} & -\frac{R_r}{\sigma L_{rr}} \end{bmatrix} \begin{bmatrix} I_{dr} \\ I_{qr} \end{bmatrix} + \begin{bmatrix} \frac{1}{\sigma L_{rr}} & 0 \\ 0 & \frac{1}{\sigma L_{rr}} \end{bmatrix} \begin{bmatrix} V_{dr} \\ V_A \end{bmatrix} \tag{36}$$

$$V_A = V_{qr} - \frac{\omega_{sl} L_m^2 \left|\overline{I_{ms}}\right|}{L_{ss}} \tag{37}$$

The active and reactive power in the coordinates system are given by

$$P_{ACT} = -\frac{3}{2}\left|\overline{V_s}\right|\frac{L_m}{L_{ss}} I_{qr} \tag{38}$$

$$Q_{REA} = \frac{3}{2}\left(\frac{\left|\overline{V_s}\right|^2}{\omega_o L_{ss}} - \frac{\left|\overline{V_s}\right| L_m}{L_{ss}} I_{dr}\right) \tag{39}$$

VII. ROBUST Hinf CONTROL

The stator flux oriented control is used in order to decouple the control of the active and reactive power. The proposed stator flux oriented control uses two robust and independent controllers based on direct and quadrature axis components of the rotor current, I_{dr}, and, I_{qr}, respectively.

Figure 3 depicts the block diagram representation of the control structure developed, where $I_{dr\,ref}$ and $I_{qr\,ref}$, are obtained from equations (38) and (39), respectively. The anti-windup compensator constant is adjusted in order to the resulting system, with the integral action given by the robust control regulator, is effectively not affected by saturation. The transfer functions I_{dr}/V_{dr} and I_{qr}/V_A are equals and are obtained from the space state DFIG representation, equation (36), taking into account that slip is constant.

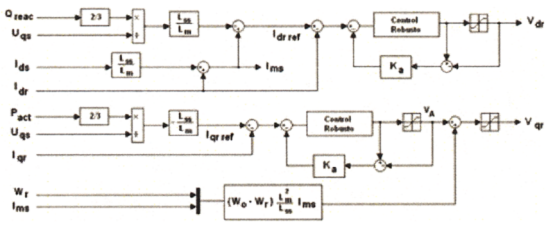

Fig. 3 Block diagram of a PI control

During the design stage the command *hinfopt* of the Robust Control Toolbox of Matlab was used. Previously, cost functions were defined to the next variables: a) error signal *(W_1)*, b) control action *(W_2)*, and the output signal *(W_3)*, equation (40).

The selection of k_i, a_i y b_i was carried out using genetic algorithms (GA), equation (41). The objective function is based on the transient response of the system when is excited with a step input, minimizing the ITSE and ISE performance indexes related with the error signal, *e(t)*, and the control action, *u(t)* respectively. *N* is the number of points, used to evaluate the transient response, at which the system reach the steady state. *t(i)* is the simulation time.

$$W_1(s) = \frac{k_1\left(s/a_1 + 1\right)}{s\left(s/b_1 + 1\right)} \quad W_2(s) = \frac{k_2\left(s/a_2 + 1\right)}{\left(s/b_2 + 1\right)} \quad W_3(s) = \frac{k_3\left(s/a_3 + 1\right)}{\left(s/b_3 + 1\right)} \tag{40}$$

$$f = 100 - \left(0{,}5\sum_{i=0}^{N} t(i) * e(i)^2 + 6{,}5\sum_{i=0}^{N} u(i)^2\right) \tag{41}$$

The following GA parameters were used: a) Crossover rate of 70%, b) Mutation rate of 0.5% c) Population size of 20. The algorithm is stopped if the standard deviation of performance function of each

individual is less than 0.01 or if maximum number of iterations is exceeded; here 500.

The speed control of the turbine is carried out using the pitch angle control technique. The control scheme is shown in figure 4. The plant model, $G(s) = {\omega_{gen}}/{\beta}$, is obtained linearizing the equation system via Taylor expansion.

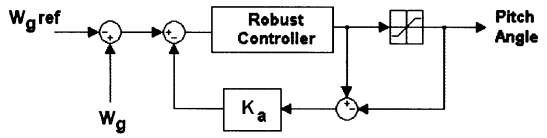

Fig. 4 Anti-windup speed robust control

The robust controller was designed again, following the steps given above, but the new objective function is defined by equation (42). The new GA parameters were: a) Crossover rate of 60% and b) Mutation rate of 0.5%, while all other parameters were kept constant.

$$f = 100 - \left(0,05 \sum_{i=0}^{N} t(i) * e(i)^{2} + 0,01 \sum_{i=0}^{N} u(i)^{2} \right) \quad (42)$$

VIII. EVALUATION OF THE PROPOSED CONTROL SYSTEM

To show the effectiveness of the proposed Hinf Robust Controller, a comparison is made with the designed PI controller with GA method [16], using the turbine NM 2000/82, manufactured by Neg Micon. The reference values correspond to the following: active power -2 MW and mechanic speed 1515 rpm.

Figure 5 shows the time response of the system using an average wind speed of 14.5 m/s and wind turbulence of 40%. Comparing the variables, the control action of the robust controller and the PI regulator are practically identical to the control loop of the mechanic speed of the shaft, but, the Hinf regulator can't follow the mechanic speed of the shaft around the rated mechanic speed of the induction generator. Otherwise, the active power remains constant during wind speed fluctuations, even though the control action V_{qr}, was increased. If the average wind speed is near to the rated speed of the turbine, 11 m/s, the response of the two controllers is practically identical, see Figure 6. Therefore, it is recommended to use the robust controller when the wind speed is greater than the rated speed of the turbine.

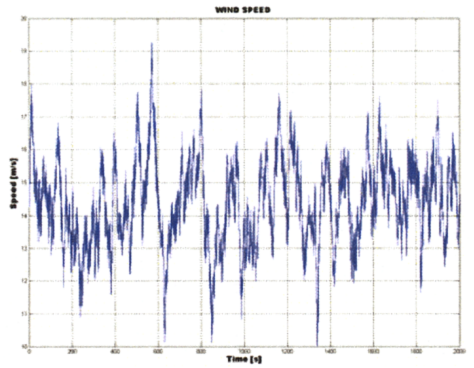

a)

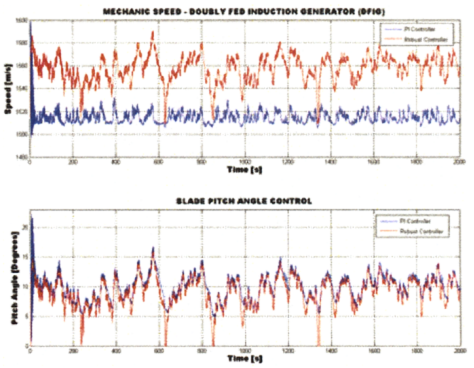

b)

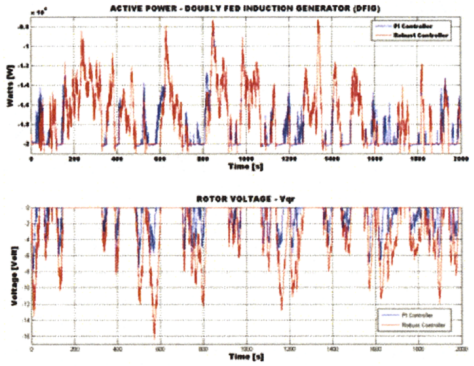

c)

Fig. 5 PI controller vs. Robust controller. a) Wind speed – 14 m/s. b) DFIG mechanic speed. c) DFIG active power.

In order to obtain the mechanical parameters of the actuator that regulates the mechanic speed of the turbine, the behaviour of the system during average wind speed variations was analyzed, taking 11 m/s and 24 m/s as the limits. Figure 7 shows that the maximum variation of the pitch angle is about 22 degrees with an angular variation of 17 degrees per minute. These characteristics are fullfilled by commercial hydraulic actuators used to control the pitch angle.

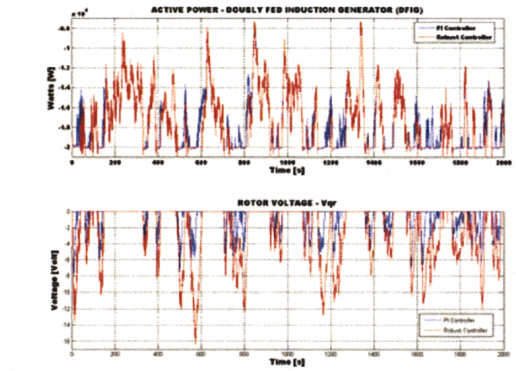

Fig. 6 Active power – Wind Speed 11 m/s

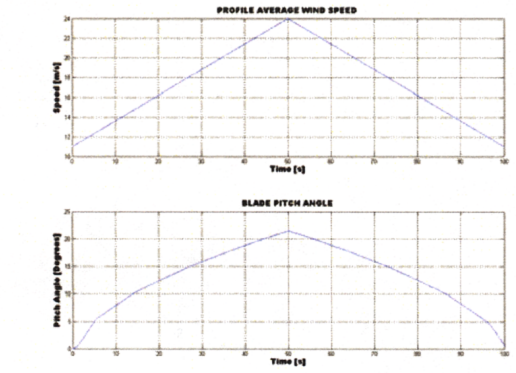

Fig. 7 Pitch angle control. a) Wind profile. b) Pitch angle

The electrical specifications to the DFIG rotor inverter can be obtained from figure 8, taking as reference an average wind speed of 24 m/s:

Voltage phase (max.)	0 to 35 V
Power	130 kW
Frequency	0 to 5 Hz

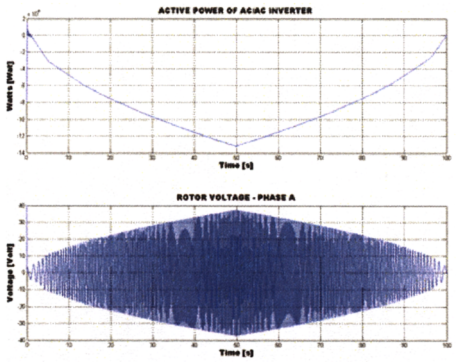

Fig. 8 AC/AC inverter a) Power flow. b) Rotor voltage

TABLA I
DFIG PARAMETERS

Frequency [Hz]	50
Stator winding resistance [Ω]	0.001
Stator winding inductance [mH]	0.07
Rotor winding resistance [Ω]	0.0013
Rotor winding inductance [mH]	0.08
Mutual inductance [mH]	3
Even number of poles	2
Moment of inertia [Kgm^2]	65

TABLA II
MECHANICAL PARAMETERS

Momento f inertia of the blades and the hub [$Kg\text{-}m^2$]	$49.5*10^5$
Low speed shaft tortional stiffness [$Kg\text{-}m^2/sg^2$]	$114*10^6$
Low speed shaft damping coefficient [$Kg\text{-}m^2/sg^2$]	10^5
High speed shaft tortional stiffness [$Kg\text{-}m^2/sg$]	$755.658*10^3$
High speed shaft damping coefficient [$Kg\text{-}m^2/sg$]	$1*10^3$
Gear box ratio	83.5

IX. CONCLUSION

An effective way to control the active power delivered by a DIFG, during high wind speed, is combining stator flux oriented control and pitch angle control. The simulation shows that the Hinf controller is more robust during variations of the wind speed compared with a PI controller, though the mechanic speed is greater than 40 rpm over the rated speed.

The performance index ISE and ITSE are a good alternative to obtain the performance function to design Hinf controllers. This allows obtain an optimal controller for each one of the three decoupled variables of the turbine dynamic model: rotor current Idr and Iqr, thus allowing to regulate the active and the reactive power and the mechanic speed of DFIG.

X. BIBLIOGRAPHY

[1] Carvalho Rosas, Pedro André. *Dynamic Influences Of Wind Power On The Power System.* PhD Thesis. Technical University of Denmark and Risoe National Laboratory. March 2003.

[2] W. Langreder. *Models For Variable Speed Wind Turbines". MsC Theses,* CREST Loughborough University and Risoe National Laboratory. 1996.

[3] Iov, Florin. *Contributions to Modelling, Analysis and Simulation of Ac Drive Systems. Application to Large Wind Turbines.* Ph.D. Thesis. Dunarea de Jos University- Galati. 2003.

[4] P. Ledesma. *Análisis dinámico de sistemas eléctricos con generación eólica.* Ph.D. Thesis. Universidad Carlos III de Madrid. 2001

[5] Paul Etienne Vidal, Maria Pietrzak David, Bernard De Fornel. *Stator flux oriented control of a doubly fed Induction machine.* Laboratoire d'Electrotechnique et d'Electronique Industrielle, Unité mixte de recherche INPT-ENSEEIHT/CNRS. 2003

[6] F. Poitiers, M. Machmoum, R. Le Doeuff, M.E. Zaim. *Control of a doubly fed induction generator for wind energy conversion systems.* Ecole Polytechnique de l'Université de Nantes, Saint Nazaire, France.

[7] Jeong-Ik Jang, Young Sin Kim, Dong Choon Lee. *Active and reactive power control of DFIG for energy conversion under unbalanced grid voltage.* Dept. Of Electrical, Eng. Yeungnam Univ. Daedong, Gyeongsan, Gyeongbuck, Korea. IEEE 2006.

[8] S. Wang, Y. Ding. *Stability analysis of field oriented doubly fed induction machine drive based on computer simulation.* Electric Machines and power systems, Vol. 21, 1993.

[9] L. Morel, H. Godfroid, A. Mirzaian, J. Kauffmann. *Double fed induction machine: converter optimisation and fiel oriented control without position sensor.* IEEE Proc. Electr. Power Appl. Vol. 145, julio de 1998.

[10] Morten H. Hansen, Anca Hansen, Torben J. Larsen, Paul Sorensen, Meter Fuglsang. *Control design for a pitch regulated, variable speed wind turbina.* Riso National Laboratory. Enero 2005.

[11] Shashitanth Suryanarayanan, Amit Dixit. *On the dynamics of th pitch control loop in horizontal axis large wind turbines.* American Control Conference, Junio 2005.

[12] Hongwei Liu, Yonggang Lin, Wei Li. *Study on Control Strategy of Individual Blade Pitch Controlled Wind Turbine.* Intelligent Control and Automation. WCICA 2006.

[13] Lars Nielsen. *Modelling and control of variable speed HAWT utilizing hybrid Control.* Aalborg University. Septiembre 2004.

[14] Rocha, Ronilson. Martins Filho, Luis Siqueira. *A multivariable $H\infty$ control for wind energy conversión system.* Department of control and Automation. Department of Computation Campus Morro do Cruzeiro. IEEE 2003.

[15] Kathryn E. Johnson, Lucy Y. Pao, Mark J. Balas, Lee J. Fingersh. *Control of variable speed wind turbines, standard and adaptive techniques for maximizing energy capture.* IEEE Control Systems Magazine. 2006

[16] González Acevedo, Hernando. Vargas Torres, Hermann Raul. *Diseño de un controlador para una turbina eólica de velocidad variable utilizando algoritmos genéticos.* II Simposio Internacional en Fuentes Alternativas de Energía y Calidad Energética. 2008

XI. BIOGRAPHIES

Hernando González Acevedo. Received the B.Sc. degree in electronic engineering from the Industrial University of Santander (UIS), Bucaramanga, Colombia, in 2000 and the M.Sc. degree in Electrical power from UIS in 2007. Currently, he is a Professor with the Electronics Engineering School at University of Santo Tomás, Bucaramanga, Colombia. His areas of interest are control, robotics, wind power generation. Mr. Gonzalez-Acevedo is a member of AMSCP (Col) Research Group on automation, modeling, simulation and control of industrial products and process. E- mail: hernando_gonza@hotmail.com

Hermann Raúl Vargas Torres. Received the B.Sc. degree in electrical engineering from the Universidad Industrial de Santander (UIS), Bucaramanga, Colombia, in 1985. The M.Sc. degree in Electrical power from UIS in 1990, and the Ph.D. degree in Electrical Engineering from Universidad Pontificia Comillas (UPCO), Madrid, Spain, in 2002.Currently, he is a Professor with the Electrical Engineering School at the Universidad Industrial de Santander (UIS), Bucaramanga, Colombia. His areas of interest are power systems stability and control, transient analysis, power quality, protective relaying, wind power and policy analysis. Mr. Vargas-Torres is a member of GISEL (Col) Research Group on Electric Power Systems. E-mail: hrvargas@uis.edu.co